AGU PUBLICATIONS

Earth and Space Science

RESEARCH ARTICLE
10.1002/2017EA000296

Key Points:
- Cloud ice particle size is an important parameter that determines cloud radiative effect, precipitation, and climate sensitivity
- A simulation experiment for a CubeSat instrument is conducted to determine the accuracy of ice particle size, humidity, and temperature retrievals
- The results show that the CubeSat instrument is capable of fulfilling the requirements of measuring ice particle size, humidity, and temperature

Correspondence to:
J. H. Jiang,
jonathan.h.jiang@jpl.nasa.gov

Citation:
Jiang, J. H., Q. Yue, H. Su, S. C. Reising, P. P. Kangaslahti, W. R. Deal, E. T. Schlecht, L. Wu, and K. F. Evans (2017), A simulation of ice cloud particle size, humidity, and temperature measurements from the TWICE CubeSat, *Earth and Space Science*, *4*, doi:10.1002/2017EA000296.

Received 17 MAY 2017
Accepted 20 JUL 2017
Accepted article online 31 JUL 2017

A simulation of ice cloud particle size, humidity, and temperature measurements from the TWICE CubeSat

Jonathan H. Jiang[1], Qing Yue[1], Hui Su[1], Steven C. Reising[2], Pekka P. Kangaslahti[1], William R. Deal[3], Erich T. Schlecht[1], Longtao Wu[1], and K. Franklin Evans[4]

[1]Jet Propulsion Laboratory, California Institute of Technology, Pasadena, California, USA, [2]Microwave Systems Laboratory, Colorado State University, Fort Collins, Colorado, USA, [3]Northrop Grumman Corporation, Redondo Beach, California, USA, [4]Department of Atmospheric and Oceanic Sciences, University of Colorado Boulder, Boulder, Colorado, USA

Abstract This paper describes a forward radiative transfer model and retrieval system (FMRS) for the Tropospheric Water and cloud ICE (TWICE) CubeSat instrument. We use the FMRS to simulate radiances for the TWICE's 14 millimeter- and submillimeter-wavelength channels for a tropical atmospheric state produced by a Weather Research and Forecasting model simulation. We also perform simultaneous retrievals of cloud ice particle size, ice water content (IWC), water vapor content (H_2O), and temperature from the simulated TWICE radiances using the FMRS. We show that the TWICE instrument is capable of retrieving ice particle size in the range of ~50–1000 μm in mass mean effective diameter with approximately 50% uncertainty. The uncertainties of other retrievals from TWICE are about 1 K for temperature, 50% for IWC, and 20% for H_2O.

1. Introduction

High-altitude ice clouds, covering more than 50% of the Earth's surface [*Wang et al*., 1996; *Wylie et al*., 2005; *Hong and Liu*, 2015; *Huang et al*., 2015], are a critically important modulator of Earth's weather and climate. They play a significant role in Earth's energy balance and hydrologic cycle through their effects on radiative feedback and precipitation and therefore are crucial for life on Earth [*Hartmann and Short*, 1980; *Su et al*., 2017]. Ice clouds trap a significant amount of thermal infrared radiation emitted from the surface and the atmosphere below the cloud, resulting in warming, referred to as the greenhouse effect. On the other hand, ice clouds reflect incoming solar shortwave (SW) radiation into space and hence also have a cooling effect. The net radiative effects of ice clouds depend on their physical characteristics, including cloud vertical structure, ice water content (IWC), and ice particle size. In particular, many studies have shown that ice particle size is extremely sensitive in determining the cloud radiative effects. For example, *Fu and Liou* [1993] showed that the radiative heating rate for a layer of ice cloud with ice water path of 30 g/m^2 would differ by a factor of 10 when the mean effective radius of its ice particles varies from 25 to 125 μm. The associated top-of-the-atmosphere (TOA) net cloud radiative forcing would change from 17 to 30 W/m^2, with longwave and SW cloud forcing differences by 77 and 90 W/m^2, respectively.

Growth of ice particle size through vapor deposition, ice multiplication, aggregation, and accretion (riming) is also crucial to precipitation, which is the most important component of the atmospheric water cycle. A key microphysical property that links ice particle size and precipitation rate is ice particle fall speed, which is typically parameterized as a power law relation with ice particle effective diameter [e.g., *McFarquhar and Heymsfield*, 1997; *Morrison and Grabowski*, 2008; *Heymsfield*, 2003; *Heymsfield and Westbrook*, 2010; *Heymsfield et al*., 2017]. However, the exact relationship between ice particle size and fall speed is not clear and may vary for different convective systems [*Heymsfield*, 2003]. The parameterizations of ice particle size and fall velocity are crucial to model simulations of severe thunderstorms [*Hong et al*., 2004] and hurricane track and intensity forecasting [*Fovell and Su*, 2007]. Without global measurements of ice particle size, estimates of precipitation from remote sensing data are subject to large uncertainties [e.g., *Bennartz and Petty*, 2001]. The retrieval of ice water content also suffers from uncertainty of a factor of 2, mostly due to the unknown ice particle size information [*Wu et al*., 2008].

It is well documented that global circulation model (GCM) simulation of high-altitude ice clouds is highly problematic [e.g., *Waliser et al*., 2009; *Li et al*., 2012; *Jiang et al*., 2012]. While the models participating in the latest assessment of the Intergovernmental Panel on Climate Change show quite consistent global average values

for cloud fraction, precipitable water, and precipitation, they exhibit widely differing average IWC vertical structures and ice water path (IWP), two fundamental quantities for cloud radiative effects and their climate feedback. Compared to simulated cloud water content and water vapor mixing ratio (H_2O) in the lower and middle troposphere, the upper tropospheric IWC and H_2O are the most problematic [*Jiang et al*., 2012; *Takahashi et al*., 2016], which points out the lack of understanding of processes governing high-altitude ice clouds and atmospheric water vapor structure. When modeled IWC is stratified by ice particle size to indicate precipitating and nonprecipitating ice particles, better agreement between the model and observation can be achieved [*Waliser et al*., 2009; *Chen et al*., 2011]. An experiment conducted by *Yang et al*. [2013] revealed that the size of detrained ice in anvil clouds effectively regulates the total precipitation, cloud longwave radiative forcing, and outgoing longwave radiation associated with deep convective clouds. A recent study by *Elsaesser et al*. [2016] further illustrates that the climate model simulated IWC error is directly linked to the unknowns in ice cloud microphysical properties, with ice particle size being the most important contributor. They demonstrated a substantial improvement in GCM-simulated IWC amount and distribution after incorporating, into the convective parameterization, a new ice particle size and fall-speed formulation derived from field campaign data sets [*Elsaesser et al*., 2016]. The results show that cloud ice particle size and fall speed are among the major GCM parameterization uncertainties in simulating the ice cloud amount and distribution that affecting climate projections. *Sanderson et al*. [2008] found that cloud ice fall velocity, and thus the ice particle size, is the second most important parameter, only behind the entrainment rate, that drives the intermodel spread in climate sensitivity. Observational constraints on ice particle size and fall speed thus have immediate impact of reducing the uncertainty of climate change predictions.

All of these findings suggest that knowledge of ice cloud properties, especially ice particle size, is important for obtaining a consistent picture of the interactions among convection, cloud radiation, and precipitation processes. The current values of ice particle size in most GCMs are prescribed empirically and remain poorly constrained. Arbitrary assumptions are made, based on our ignorance of ice microphysics, resulting in compensating errors in weather and climate models that severely undermine the fidelity of future climate predictions [*Bony et al*., 2006; *Golaz et al*., 2013].

Currently, NASA's A-Train satellites [*L'Ecuyer and Jiang*, 2010] provide limited ice cloud particle size information. CloudSat 94 GHz radar is mostly sensitive to particles larger than ~600 μm in diameter, while Moderate Resolution Imaging Spectroradiometer mainly detects cloud top particle effective radii smaller than ~50 μm [*Buehler et al*., 2007; *Jiang et al*., 2011]. However, as shown by in situ measurements, the number density of ice particles often peaks at particle sizes between 100 and 1000 μm in effective diameter, especially for ice clouds formed by convection and stratiform ice clouds at temperatures warmer than −40°C [*Heymsfield et al*., 2013]. New spaceborne instruments need to be developed to fill this measurement gap in ice particle size. This paper will demonstrate a retrieval simulation package for a compact multifrequency millimeter- and submillimeter-wave length CubeSat instrument, Tropospheric Water and cloud ICE (TWICE) [*Reising et al*., 2016; *Kangaslahti et al*., 2016] that can provide cloud ice particle size information between ~50 μm and ~1000 μm, together with IWC, atmospheric temperature (T), and H_2O information simultaneously. TWICE has been developed under the 2013 Instrument Incubator Program funded by the NASA Earth Science Technology Office. It is a wideband, multifrequency (118, 183, 240, 310, 380, and 670 GHz) instrument focusing on measurements of cloud IWC and ice particle size, together with H_2O, T, and relative humidity (RH). For ice particle size retrieval, wideband channels at 240, 310, and 670 GHz, far from absorption line centers, are selected by TWICE since these frequencies have atmospheric transmission characteristics similar to window channels. Such submillimeter-wave channels have been shown to be directly related to ice mass and ice particle size [*Evans et al*., 1998].

A CubeSat is a miniaturized satellite that is made up of multiples of $10 \times 10 \times 10$ cm^3. Each such cube is called 1U. As a candidate instrument for future CubeSat missions, TWICE has a 3U × 2U form factor, i.e., a 6U CubeSat. Depending on the mission design, TWICE can fly as a 6U CubeSat or a single spacecraft payload on a near-polar orbit or near-equatorial orbit. It can also be a 6U CubeSat deployed from the International Space Station (ISS), or an instrument attached to ISS, orbiting near 400 km altitude and 51.6° inclination. TWICE is designed to be conically scanning, viewing the Earth over an azimuth angle range of approximately 100° and a fixed Earth incidence angle of approximately 45°. The field of view (FOV) depends on TWICE's orbital altitude. For a nominal 400 km altitude orbit, the FOV at the surface is estimated to be about 10 km × 15 km. For the simulations conducted in this paper, we assume nadir viewing and a FOV of

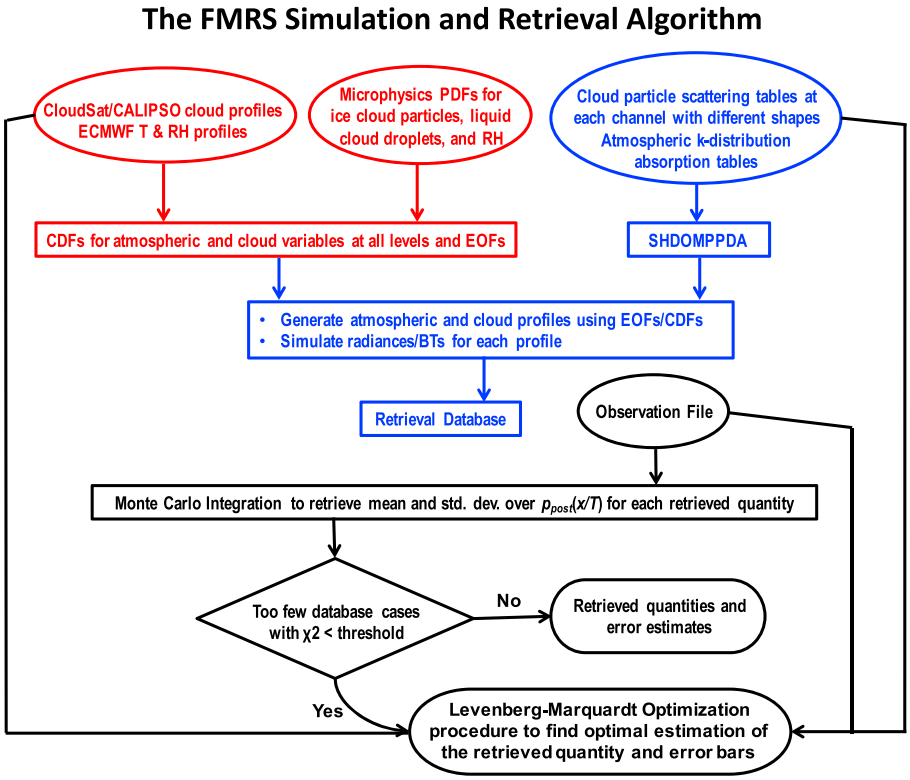

Figure 1. Flowchart of FMRS simulation and retrieval algorithm, which consists of three main components. The first component generates the a priori information (red), the second component computes the retrieval database based on the a priori profiles and a radiative transfer model (blue), and the third performs the Bayesian retrieval using the MCI and LMO methods (black).

20 km × 20 km, consistent with the horizontal resolution of the "truth" file used in the simulation (see later discussions in section 3.2).

This paper presents a detailed simulation of these fundamental radiance measurements from TWICE and assesses the accuracy of its retrievals. The description of the simulation and retrieval algorithm is given in section 2. The forward model simulation, simulated retrieval, and uncertainty estimates are presented in section 3. A summary and conclusion are given in section 4.

2. The Forward Radiative Transfer Model and Retrieval System

The forward radiative transfer model and retrieval system (FMRS) we adopted for TWICE uses a Bayesian methodology [*Evans et al*., 2002; *Evans et al*., 2012] to retrieve the key parameters describing both the atmosphere and cloud hydrometers. These parameters include vertical profiles of IWC, ice particle equivalent sphere effective diameter (D_e), T, H_2O (or RH) and vertically integrated cloud parameters including IWP, column mass-mean effective diameter (D_{me}), and cloud median mass height (Z_{me}). Ice particle shape mixtures are among the most difficult quantity to measure and retrieve from observations. The current FMRS includes single-scattering properties for four different realistic ice particle shapes (hexagonal plate aggregates, sphere aggregates or graupel, dendrite aggregates, and solid spherical hail). Previous studies pointed out that relative fractions and single-scattering properties of these four shapes are consistent with in situ measurements of tropical ice clouds and greatly improve the accuracy of simulated microwave brightness temperatures [*Evans et al*., 2012].

Figure 1 shows the flowchart of the FMRS algorithm, which consists of three main components. The first generates the a priori information (red), the second computes the retrieval database based on the a priori profiles and a radiative transfer model (blue), and the third performs the Bayesian retrieval using a hybrid

Monte Carlo integration (MCI) [*Kroese et al*., 2011] and Levenberg-Marquardt optimization (LMO) approach (black) [*Levenberg*, 1944; *Marquardt*, 1963].

There are four major advantages of the FMRS. First, it is highly computationally efficient. Since the retrieval database is precomputed, there is no need to perform a radiative transfer calculation for each new observation. Second, it introduces the a priori in a clearly defined manner by using cumulative distribution functions (CDFs) and empirical orthogonal functions (EOFs) for *T*, RH, and cloud parameters at multiple layers of the atmosphere. The CDFs capture the complete single-point statistics of all of the atmospheric and cloud parameters for a wide variety of ice clouds, while the EOFs capture the relationships among different parameters and different layers. As a result, the FMRS algorithm covers a complete and realistic spectrum of the atmosphere and cloud with parameters covarying with each other. Third, a large number of millimeter- and submillimeter-wave frequencies have been incorporated into the FMRS algorithm covering 100 to 900 GHz, which facilitates the need for a unified retrieval algorithm for a variety of millimeter wavelengths and other millimeter-wave instruments. Lastly, instead of assuming particular ice particle shape distributions, the FMRS algorithm treats particles as a mixture of different shape categories with varying mixing fractions, allowing for improved simulations of microwave radiative transfer in ice clouds. This FMRS algorithm has been successfully tested and validated with data collected by multiple submillimeter-wave radiometers during multiple field campaigns, such as the Conical Scanning Submillimeter-wave Imaging Radiometer and the Far Infrared Sensor for Cirrus [*Evans et al*., 2012].

One of the key parameters, the ice particle size distribution, is defined by the D_e. The column-integrated value of particle size, D_{me}, is the mass weighted (or IWC weighted) mean D_e, and the width of the size distribution is measured by the D_e dispersion, $D_{e,\mathrm{disp}}$:

$$\begin{aligned} D_{me} &= \frac{\int N(D_e) D_e^3 D_e dD_e}{\int N(D_e) D_e^3 dD_e} \\ D_{e,\mathrm{disp}} &= \frac{1}{D_{\mathrm{me}}} \left[\frac{\int N(D_e) D_e^3 (D_e - D_{\mathrm{me}})^2 dD_e}{\int N(D_e) D_e^3 dD_e} \right]^{1/2} \end{aligned} \tag{1}$$

The FMRS algorithm simulates cloud layers containing both ice particles and liquid cloud droplets. Ice particles are specified by IWC, D_{me}, Z_{me}, and $D_{e,\ \mathrm{disp}}$, with a mixture of different ice particle shapes. Liquid cloud droplets are specified by liquid water content (LWC), D_{me}, and a fixed D_e dispersion ($D_{e,\mathrm{disp}}$ = 0.3). Below the freezing level, the mass of the melted ice particles is also included because of the substantial sensitivity of frequencies near 118 GHz and 183 GHz to these hydrometers using a simple melting model described in *Evans et al*. [2012]. For each of these cloud particle types, the a priori information is included in the FMRS algorithm together with the atmospheric conditions.

The principle of the FMRS retrieval algorithm is Bayes' theorem of probability theory:

$$p_{\mathrm{post}}(\boldsymbol{x}|\boldsymbol{T}) = \frac{p_f(\boldsymbol{T}|\boldsymbol{x}) p_{\mathrm{prior}}(\boldsymbol{x})}{p_{\mathrm{prior}}(\boldsymbol{T})} \tag{2}$$

where $\boldsymbol{x}$ and $\boldsymbol{T}$ are the vectors of cloud and atmospheric parameters and measured radiances or brightness temperatures (BTs), respectively. The prior probability distribution functions (PDFs), $p_{\mathrm{prior}}(\boldsymbol{x})$, represent our knowledge of the atmospheric state before taking the measurements, providing the a priori profiles for the retrieval. The conditional PDF, $p_f(\boldsymbol{T}|\boldsymbol{x})$, is the distribution of BTs or radiances given an atmospheric state calculated by forward radiative transfer models. Currently, the Spherical Harmonics Discrete Ordinate Method for Plane-Parallel Data Assimilation (SHDOMPPDA) [*Evans*, 2007] model is used, with options available for other radiative transfer models. The resulting conditional posterior PDF $p_{\mathrm{post}}(\boldsymbol{x}|\boldsymbol{T})$ gives the distribution of the vector $\boldsymbol{x}$ given the measured *T*. The retrieval is then performed by integrating $p_{\mathrm{post}}(\boldsymbol{x}|\boldsymbol{T})$ to find the posterior PDF weighted mean parameter vector $\boldsymbol{x}_{\mathrm{ret}}$ together with the weighted standard deviation as the retrieved uncertainty:

$$\begin{aligned} \boldsymbol{x}_{\mathrm{ret}} &= \int \boldsymbol{x} p_{\mathrm{post}}(\boldsymbol{x}|\boldsymbol{T}) d\boldsymbol{x} \\ \sigma_x^2 &= \int (\boldsymbol{x} - \boldsymbol{x}_{\mathrm{ret}})^2 p_{\mathrm{post}}(\boldsymbol{x}|\boldsymbol{T}) dx \end{aligned} \tag{3}$$

Table 1. Center Frequencies, Offsets, and Bandwidths of the TWICE Channels

Channel	Center Frequency	±Offset Frequency	Bandwidth
1	118.75	1.1	0.4
2	118.75	1.5	0.4
3	118.75	2.1	0.8
4	118.75	5.0	2.0
5	183.31	1.0	0.5
6	183.31	3.0	1.0
7	183.31	6.6	1.5
8	243.20	2.5	3.0
9	310.00	2.5	3.0
10	380.20	0.75	0.7
11	380.20	1.80	1.0
12	380.20	3.35	1.7
13	380.20	6.20	3.6
14	664.00	4.20	4.0

Since the database cases are distributed according to the prior PDF, the MCI method simplifies the Bayes integral in (3) for the retrieved vector to be a summation over cases that match the observation:

$$x_{\text{ret}} = \frac{\sum_i x_i \ \exp\left(-\frac{1}{2}\chi_i^2\right)}{\sum_i \exp\left(-\frac{1}{2}\chi_i^2\right)}, xi \text{ from } p\text{prior } (\boldsymbol{x}). \tag{4}$$

A similar summation over database cases for σ_x yields the uncertainty in the retrieval. If there are not enough MCI database points below a threshold value of χ^2, the LMO approach is used to retrieve that specific vector following the framework described in *Rodgers* [2000], and χ^2 is given by

$$\chi^2 = \sum_{j=1}^{N} \frac{\left(T_j^{\text{sim}} - T_j^{\text{obs}}\right)^2}{\sigma_j}, \tag{5}$$

T_j^{sim} and T_j^{obs} are the simulated and measured observations in channel j, respectively, with a combined measurement and forward modeling uncertainty of σ_j. N is the number of channels.

An important feature of the FMRS algorithm is the CDF/EOF a priori information. This framework combines rich vertical profiles of clouds and atmosphere measured from satellites with detailed in situ microphysical measurements. Expressing the Bayesian prior PDF in terms of CDF allows for arbitrary distributions, while the EOFs provide the crucial correlations among key parameters. The primary data sources for this a priori are CloudSat radar reflectivity profiles, Cloud-Aerosol Lidar and Infrared Pathfinder Satellite Observation (CALIPSO) lidar cloud fraction for each CloudSat range bin, and the corresponding European Centre for Medium-Range Weather Forecasts (ECMWF) profiles of T and RH. The CALIPSO data allow the prior to have lower IWC and D_{me} values, to which CloudSat has limited sensitivity. The cloud microphysical probability distributions are based on in situ aircraft measurements of clouds and ambient conditions together with the size dependence of particle shapes. Combining these data sets, stochastic profiles of IWC/LWC, D_{me}, and $D_{e,\text{disp}}$ for ice and liquid hydrometers are generated for each CloudSat radar profile with ECMWF atmospheric profiles. Both the CDFs and the EOFs for various parameters at multiple layers of atmosphere are constructed as the a priori for the retrieval, which also serves as the basis for the retrieval database after the forward radiative transfer calculations.

3. Results

Using the FMRS, forward simulations and retrievals are performed to determine the accuracy of retrieved cloud, humidity, and temperature parameters with the 14 TWICE frequency channels listed in Table 1. A tropical atmospheric state simulated by the Weather Research and Forecasting (WRF) model is used to illustrate a "real" case of TWICE observations and retrievals.

Table 2. Ice Particle Shapes Used in the Simulation and Their Applied Ranges of D_{me}

Particle Shape	Min D_{me} (μm)	Max D_{me} (μm)
Plate aggregates	6.310	398.1
Sphere aggregates	5.012	1584.9
Snow aggregates	63.10	1584.9
Solid sphere	398.1	3162.3

3.1. The A Priori Database, Weighting Function, and Radiance Sensitivity to Particle Size

The first step is to build the a priori database. In the current simulation, the CDF/EOF file is produced from aircraft measurements taken during the NASA Tropical Composition, Cloud and Climate Coupling (TC4) field campaign and from CloudSat/CALIPSO measurements along 41 orbits that intersected the region from 4°N to 12°N and 90°W to 80°W in July and August 2007, coincident with the TC4 experiments. A total of 32,403 radar columns are used, along with three stochastic hydrometeor profiles generated for each radar column. The a priori IWC profiles have a large range from effectively clear ($<10^{-5}$ g/m^3) to about 10 g/m^3, and D_{me} ranges from below 15 μm to above 1500 μm, which facilitates the retrieval simulation over a wide range of ice clouds. The four different shapes listed in Table 2 are considered in the ice particle scattering properties, such that the mixture of these realistic shapes can model the millimeter-wave radiative properties of ice clouds in the tropical convective core, stratiform region, and cirrus anvils, which are the objectives of TC4 measurements used in this simulation test. Simple a priori information between ice particle shape and D_{me} is used (Table 2) to adjust the mixing fractions of the variety of shapes, which are determined from the TC4 measurements. This shape and size information is also used to construct the single-scattering property tables for ice particles at each TWICE frequency channel as a function of D_{me}, D_e dispersion, particle shape, and temperature, which are then used in the SHDOMPPDA radiative transfer calculation in the cloudy atmosphere.

A database of 10^6 cases is generated stochastically from the spectrum of statistics in the a priori CDF/EOFs. This database includes both atmosphere and cloud hydrometer profiles and the TOA brightness temperature spectra. The atmosphere and cloud profiles are input into the SHDOMPPDA with the specification of TWICE frequency channels to calculate the TOA brightness temperature with the single-scattering property tables generated previously. For retrievals in other regions, spatially and temporally dependent a priori databases can be easily constructed with the algorithm.

To estimate the sensitivity of TWICE frequency channels to the ice particle size, we also add the uncertainty of 1 K to each channel, which includes both the measurement noise and radiative transfer error. Current estimates of the measurement noise of TWICE channels are on the order of ~6×10^{-1} K. Radiances near the water vapor absorption lines at 183 and 380 GHz were chosen to measure H_2O profiles. The weighting functions of these water vapor absorption lines are shown in Figures 2a and 2b for the channels near the 183.31 GHz and 380.20 GHz absorption lines, respectively. Atmospheric temperature profiles are obtained using frequencies near the oxygen absorption line at 118.75 GHz. The weighting functions for the channels near the 118.75 GHz absorption line are shown in Figure 2c. Figures 2d, 2e, and 2f show the weighting functions at the window channels near the 240 GHz, 310 GHz and 664 GHz ozone lines for cloud measurements, respectively. The solid lines correspond to the weighting functions for clear conditions, while the dashed lines are for cloudy calculations using the same atmospheric T and H_2O profiles with ice cloud layers present between 6 and 15 km. The difference between the clear and cloudy calculations clearly shows the impact of clouds on the transmittance, and hence the TOA brightness temperature. The magnitude of such impact depends on channel specifications and cloud properties, as shown in Figure 3.

The cloud ice water content and particle size retrievals rely on radiance measurements from all TWICE frequency channels. At these millimeter-wave and submillimeter-wave frequencies, the upwelling radiation from the lower troposphere below the high cloud freezing level is quite large. The interaction of ice clouds with the upwelling radiation is mostly by scattering. Therefore, the near nadir observation of ice clouds at these frequency channels is based on the reduction in measured brightness temperatures in the presence of ice particles as compared to the clear-sky case [*Wu et al.*, 2006; *Buehler et al.*, 2007]. The radiance measurements are quite sensitive to ice particle size. As ice particle size increases from much smaller than to the order of the wavelength of the radiometer's frequency range, there is a transition in scattering mechanisms from Rayleigh to Mie scattering.

To demonstrate the dependence of brightness temperature difference due to ice particle scattering at different ice particle sizes, we conducted a sensitivity study using 10^6 cases in the retrieval database for a cloudy-sky simulation, in which the atmospheric temperature and water vapor profiles, together with vertical profiles

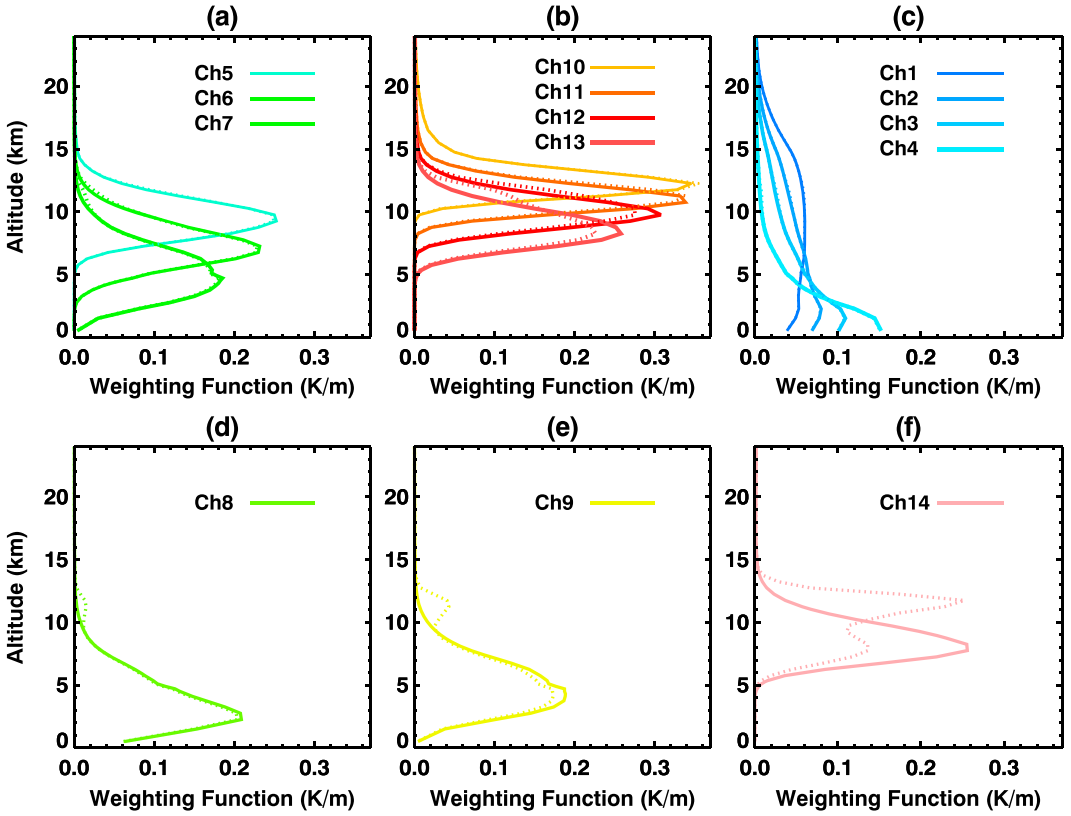

Figure 2. (a) Weighting functions versus altitude at TWICE channels near the 183.31 GHz water vapor line. (b) Weighting functions versus altitude at TWICE channels near the 380.20 GHz water vapor line. (c) Weighting functions versus altitude at TWICE channels near the oxygen line at 118.75 GHz. (d–f) Weighting functions versus altitude at window channels near the 240 GHz, 310 GHz, and 664 GHz ozone lines, respectively. The solid lines are for clear sky, and the dotted lines are for cloudy scenes.

of IWC and D_e, are input to the SHDOMPPDA radiative transfer model to calculate the TOA brightness temperature at the 14 TWICE frequency channels. A clear-sky simulation was also conducted, in which radiative transfer calculations were performed with the same atmospheric profiles but by setting IWC to zero. In both sets of calculations, a nadir viewing angle is used. Figure 3 shows the cloud-induced changes of brightness temperature due to ice particle scattering, as a function of IWP on the y axis and D_{me} on the x axis. All TWICE channels are sensitive to changes of IWC and D_{me}, but as channel frequencies increase, greater sensitivity to smaller D_{me} can be seen. The three window channels chosen around the 243, 310, and 664 GHz ozone lines are the most sensitive to ice cloud variations. With current channels, only limited sensitivity is observed for $D_{me} < 50$ μm. Significant ice particle sensitivity is also shown at the TWICE frequency channels farthest from the absorption line centers. These wide channels are selected because their atmospheric transmission characteristics are similar to window channels. The sensitivity to ice particle scattering is diminished at frequencies below the 118.75 GHz water vapor absorption line. At the upper frequency limit, above 664 GHz the opacity of the atmosphere due to water vapor masks most of the signal from the ice clouds, and therefore, this submillimeter wave frequency band is uniquely useful for this measurement [*Buehler et al.*, 2007]. Measurements at all of these TWICE frequency channels can be used to quantify information about the ice particle size distribution.

Simulation experiments are carried out to show the uncertainty range of the retrieval. Ten thousand cases are generated randomly from the a priori as the test database, and retrievals are performed for this test database using the previously generated retrieval database. Statistics are built up on the results for the 10,000 cases and are shown in Figure 4, in which the retrival errors are the standard deviations of the retrieval bias with respect to observed data ("truth") in the test database. Figure 4a shows the retrieval errors (in %) as a function of IWP. Errors of less than 20% are found for IWP values ranging from about 50 to 1000 g/m$^{2.}$ As expected,

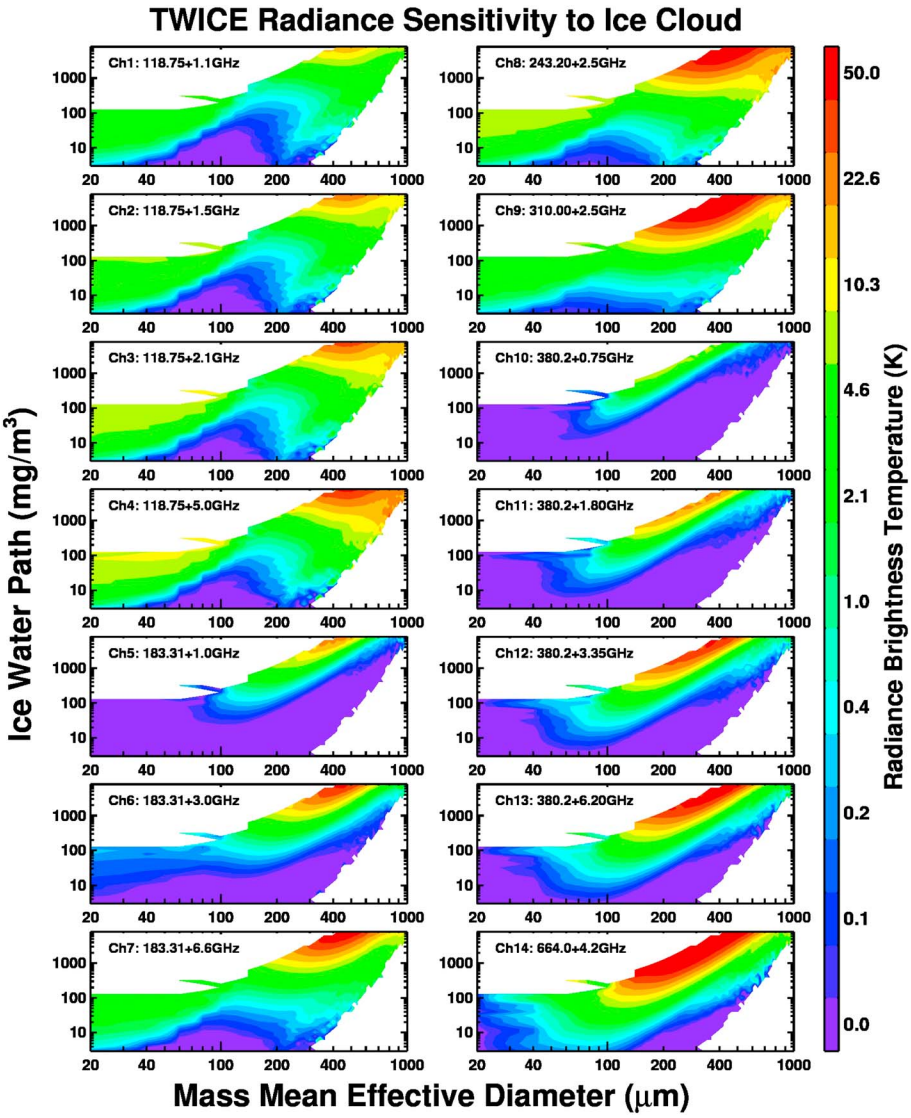

Figure 3. The FMRS simulated radiance brightness temperature differences due to ice particle scattering at 14 TWICE frequency channels as a function of IWP and D_{me}.

larger errors are also found for lower IWP values because of the smaller radiance signature of these hydrometeors. The retrieval errors increase to 40% at the large end of the IWP range (~10^4 g/m^2). This happens because the radiances begin to saturate at high IWP, and the number of cases with IWP >1000 g/m^2 accounts for less than 10% of the database. Similarly, when the relative errors are plotted as function of D_{me} in Figure 4b, the range with less than 40% error in IWP is at D_{me} values larger than about 50 μm. Figure 4c shows the relative errors as a function of mass weighted cloud height, Z_{me}. The submillimeter-wave channels are relatively insensitive to very cold cirrus, which have small particles and low IWPs. On the other hand, water vapor absorption reduces the sensitivity of higher-frequency channels to clouds at lower altitudes. As a result, the IWP error is larger than 20% for cloud with Z_{me} smaller than 8 km or greater than 14 km. These results shown in Figure 4 represent the statistics of TWICE retrieval errors.

3.2. A Simulated TWICE Retrieval Scenario and Uncertainty Estimates

To simulate TWICE retrieval under a "real" case scenario, we use a "truth" that covers a realistic distribution of cloud and atmospheric parameters to generate radiances to be observed by TWICE. For that, 251 profiles along the latitude of 15°N band between longitudes of 140°W and 90°W are taken from the WRF simulated

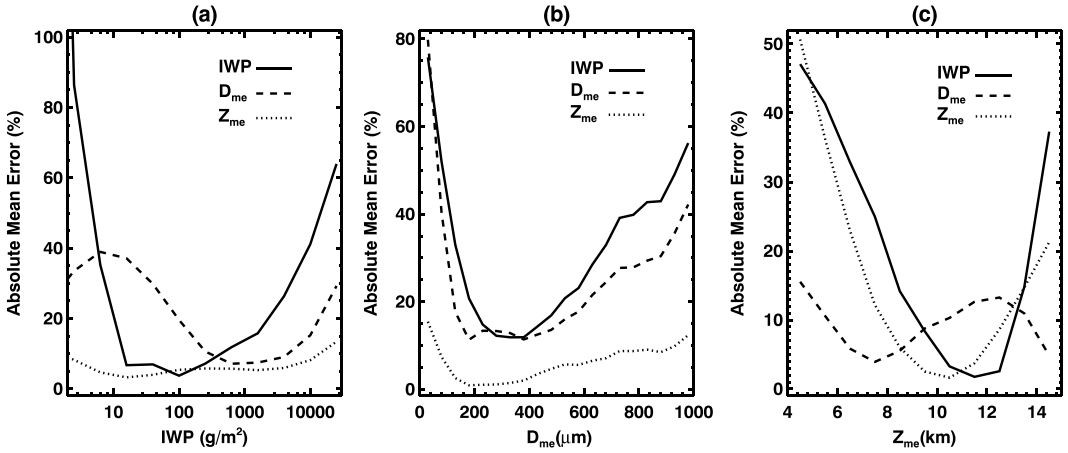

Figure 4. The median absolute fractional error of the retrieved IWP, D_{me}, and Z_{me} as (a) a function of IWP, (b) as a function of D_{me}, and (c) as a function of Z_{me}.

fields. These profiles include the vertical structures of T, H_2O, RH, IWC, and liquid water content (LWC), as well as the D_e of ice and liquid cloud particles. The WRF model we used is the Pacific Northwest National Laboratory-updated WRF V3.5.1 [*Skamarock et al.*, 2008]. The model runs at 0.2° horizontal resolution covering an area of 60°S–60°N, 180°W–60°W, with 50 levels in the vertical. The model simulation begins at 0000 UTC on 31 May 2007. We used the simulation's output at 0000 UTC on 1 June 2007. The initial and boundary conditions are taken from the ERA-Interim (http://rda.ucar.edu/datasets/ds627.0/). The physical parameterizations include the New Simplified Arakawa-Schubert scheme [*Han and Pan*, 2011] for convective processes, the Yonsei University scheme [*Hong et al.*, 2006] for planetary boundary layer processes, the Morrison 2-moment scheme [*Morrison et al.*, 2009] for cloud microphysics, and the Rapid Radiative Transfer Model for General circulation model schemes for shortwave and longwave radiations [*Iacono et al.*, 2008]. The WRF-simulated ice particle effective radius is computed based on the formula derived from measurements in tropical anvils reported by *McFarquhar and Heymsfield* [1997]. Precipitation is included in the simulation by assuming that rainwater consists only of melted ice particles and that the raindrop size is 1 mm. The size of these particles is determined using the ratio between the ice and rainwater content in a given layer, assuming that rainwater is distributed uniformly in the vertical direction. Since neither the ice particle shape nor size distribution information is readily available from the WRF-simulated atmosphere and cloud, simplifying assumptions are made in the retrieval simulations. Ice particle shapes are assumed to be equally composed of different shapes when the particle size is in the applied ranges given in Table 2. Particle size dispersion is assumed to be 0.30 for both ice and liquid clouds.

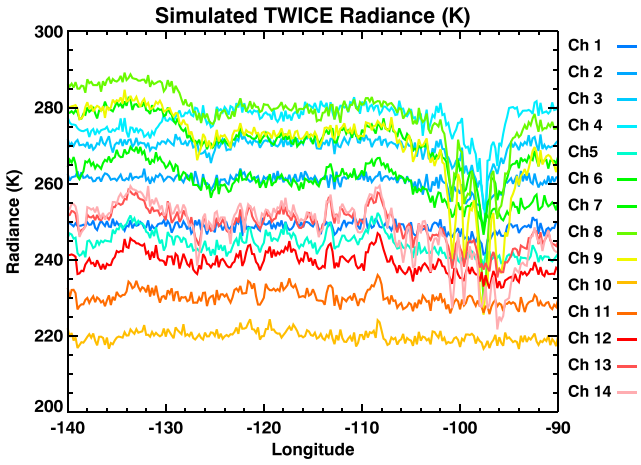

Figure 5. The FMRS simulated radiances as "seen" by the TWICE frequency channels. TWICE channel numbers are defined in Table 1.

Figure 5 shows the simulated TWICE radiance (or brightness temperature) observations for the 251 "true" atmospheric profiles, which are calculated with the FMRS's SHDOMPPDA radiative transfer model with added noise of 1 K to each frequency channel. TWICE "flying" from 90°W to 140°W along the 15°N latitude band with nadir viewing angle is assumed in the FMRS simulation. TWICE's horizontal FOV in this case is 20 km × 20 km, consistent with the 0.2° horizontal resolution of the "truth" file from WRF.

These simulated TWICE radiance observations are then input into the FMRS Bayesian algorithm for retrieval, and

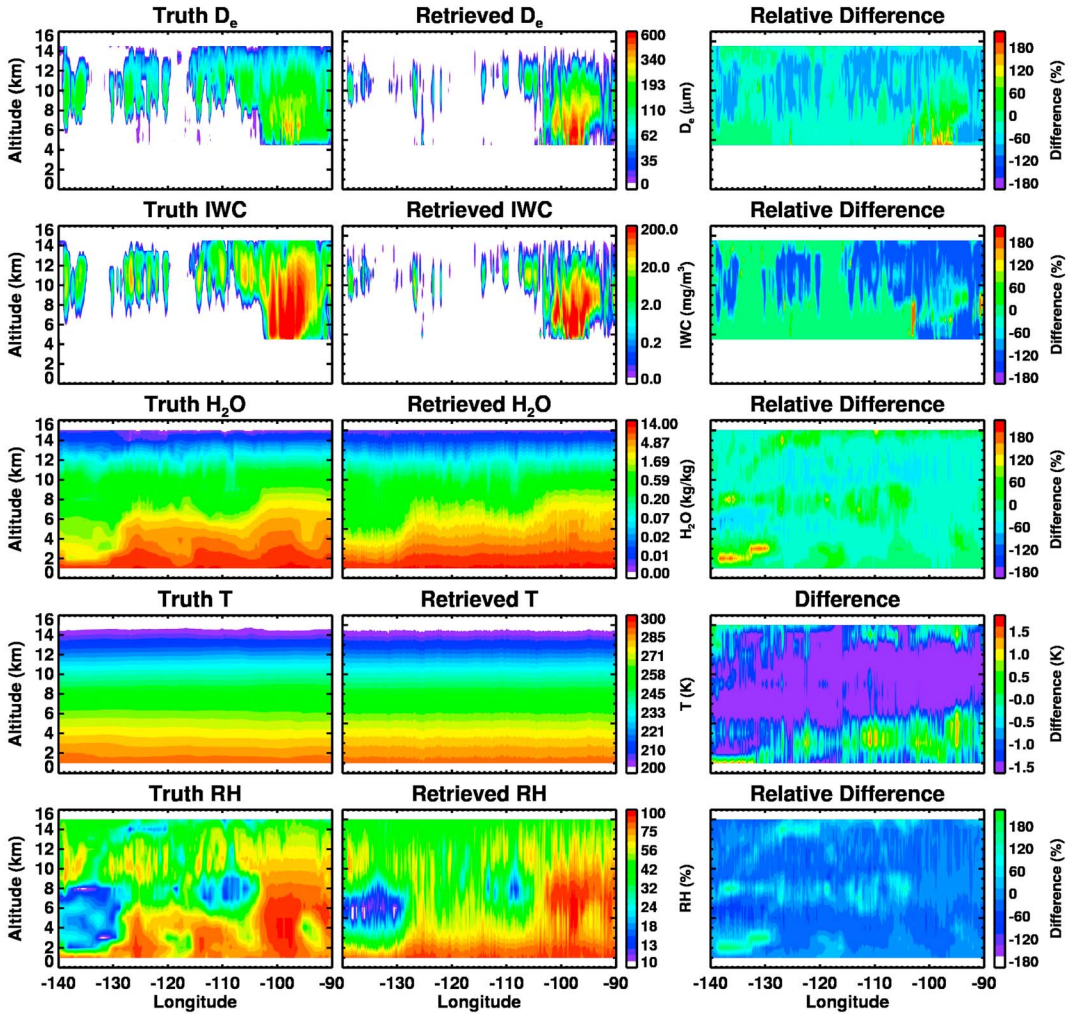

Figure 6. (left column) The vertical profiles of D_e, IWC, H_2O, T, and RH along the latitude of 15°N band between longitudes of 140°W and 90°W from WRF simulations, which are used as "truth". (middle column) The retrieved profiles of the same parameters from the FMRS retrieval algorithm for TWICE. (right column) The relative differences, in percent, computed as the retrieved values minus the truth values and then divided by the truth values. Differences for temperature are shown in K due to the low percentage values.

results are compared with the "truth", as shown in Figure 6 for D_e, IWC, H_2O, T, and RH profiles, respectively. Compared with the "truth", the overall agreement is quite good, although the retrieved profiles are less continuous in time due to mismatched field of view related to sampling frequency. The mean retrieval errors compared with the truth profiles are summarized in Figure 7.

Figures 6 and 7 both illustrate the performance and accuracy of the FMRS retrieval for TWICE. Retrieval errors are obtained from the comparison between the retrieval and the initial WRF states and are quantified as the difference between the two (retrieval–"truth"). Both the case-by-case difference (Figure 6) and the mean bias of all the cases (right column, Figure 7) are presented. The D_e and IWC profiles are limited to altitudes above the freezing level at ~5 km. The D_{me} retrievals have low biases in the upper level cirrus but show high biases in the convective core below ~8 km. The mean retrieval for D_e is within ~50%. The IWC retrievals have an overall low bias, but overall, the mean bias is within ~50%.

The H_2O retrievals perform very well above 8 km with mean biases less than 20%. In the lower troposphere, the retrieval has poorer performance in capturing the small horizontal variation features resulting, in this case, in low bias at ~4–6 km and high bias below 4 km. Overall, H_2O retrieval error, however, stays within ~25%. For T, the mean retrieval error is within 1 K in the lower troposphere below ~5 km but has up to 3 K

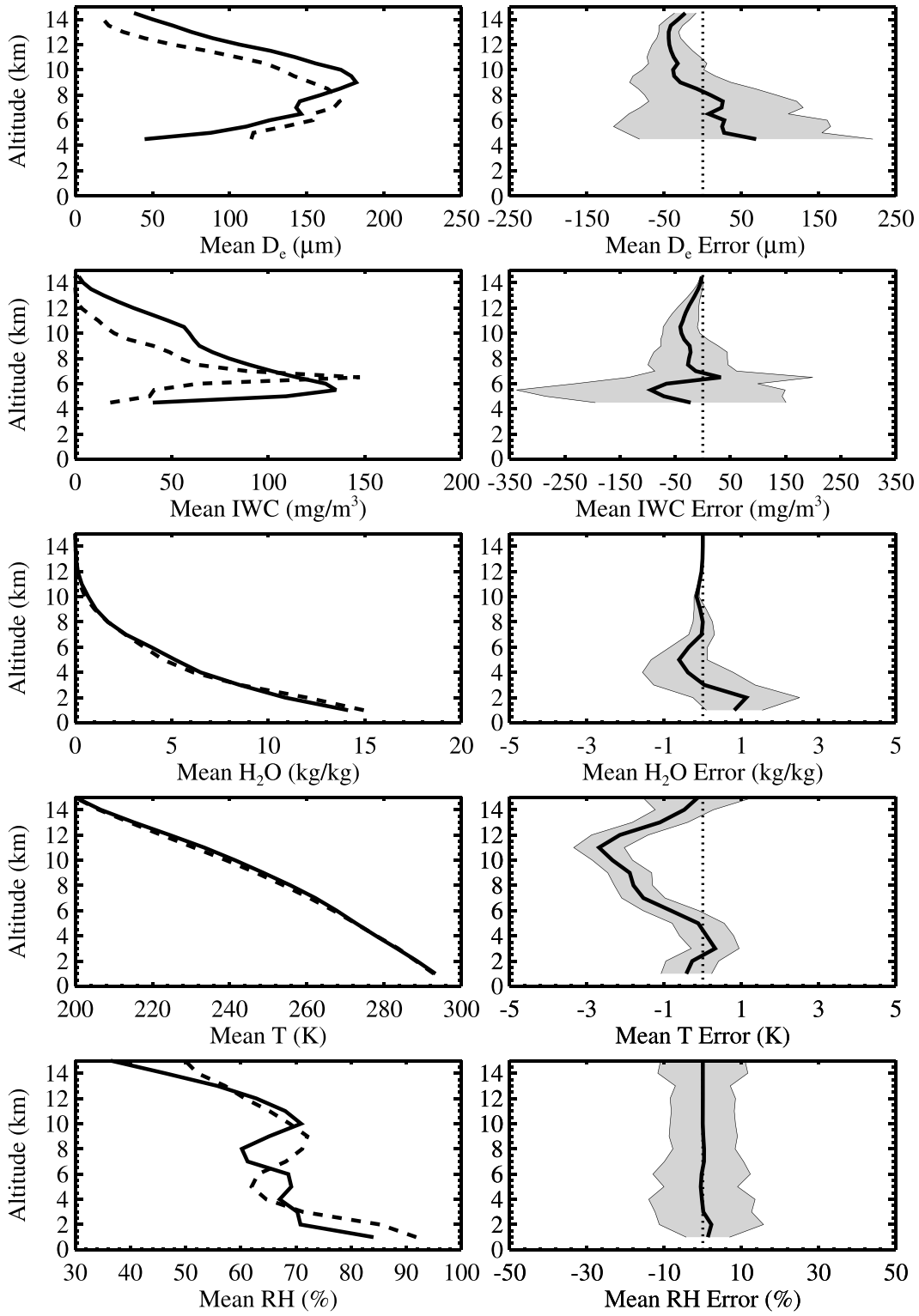

Figure 7. (left column) The mean truth (solid line) and mean retrieved (dashed line) profiles of D_e, IWC, H_2O, T, and RH. (right column) The mean error and RMS error of the mean profiles.

cold bias in the troposphere. The RH retrieval performs well at all altitudes but is missing detailed variations in the lower troposphere due to the limited sensitivity of the water vapor sounding channels in the tropical atmosphere. The mean RH biases are within ~40%.

Although the FMRS enables TWICE to provide vertical distributions of retrieved quantities, the errors in the retrieved profiles depend on both the weighting functions and a priori information on the properties of the sought profile. The weighting function at a specific height indicates how sensitive the measurement at the top of the atmosphere is at that height level, and the vertical width of the weighting function defines the vertical resolution. The shapes of the weighting functions indicate that the vertical resolutions for TWICE measurements are typically coarse at ~3 to 5 km. The a priori information requires that the retrieved quantity remains with a predefined range or provides the relationship among different quantities. For the FMRS, the a priori information is provided by the ECMWF reanalysis, combined with CDF/EOF information from CloudSat/CALIPSO observations and TC4 field campaigns, which is independent of the WRF simulation from which the "truth" data are obtained. Since most restrictions of this practice could inevitably lead to systematic retrieval error, proper validation of both WRF model and actual TWICE measurements after launch is required.

4. Summary and Conclusion

This paper describes and demonstrates a forward radiative transfer model and retrieval system (FMRS) to simulate and simultaneously retrieve, from the TWICE CubeSat measurements, cloud ice parameters, including effective diameter (D_e), ice water content (IWC), water vapor mixing ratio (H_2O), temperature (T), and relative humidity (RH) profiles, as well as the column-integrated quantities ice water path (IWP), mass-mean effective diameter (D_{me}), and cloud median mass height (Z_{me}). The paper discusses important scientific needs for such measurements. Retrieval experiments using the FMRS are performed using the TWICE millimeter- and submillimeter-wave channels to determine the accuracy of retrievals from TWICE's measurements.

To simulate the TWICE observation and retrieval, the following steps are performed: (1) We first use a WRF model to generate a model atmosphere with the associated parameters including D_e, IWC, H_2O, T, and RH, which are referred to as "truth". (2) These "truth" parameters are used as input to the FMRS's radiative transfer model to produce the radiances as the simulated TWICE "observations". (3) The retrieval calculations are then performed by the FMRS using the simulated TWICE radiances as input, and the "retrieved" parameters of D_e, IWC, H_2O, T, and RH are produced.

Our analyses show that TWICE is capable of retrieving D_e of 50–1000 μm range with better than 50% uncertainty, which fills the existing gap in ice cloud particle sizes between currently available spaceborne remote sensing modalities. We also demonstrate that TWICE has the ability of simultaneously retrieving IWC, H_2O, and RH with better than about 50%, 20%, and 40% uncertainties, respectively, and T with uncertainty of ~1 K.

Based on the simulated capability presented in this paper, TWICE shall provide, for the first time, global measurements of ice cloud particle effective diameter profiles. The associated ice water amount, humidity, and temperature profiles will also be provided. The estimated uncertainties for each measurement are smaller than the differences between current climate model results and existing observations as well as intermodel differences [*Jiang et al.*, 2012]. The ice cloud particle size profiles will enable significant advances in fundamental understanding of cloud microphysical and precipitation processes, cloud radiative forcing, and feedback, thereby improving our predictive capabilities in extreme weather, water cycle, and climate change in response to increasing greenhouse gases.

Acknowledgments
This work was supported in part by the U.S. National Aeronautics and Space Administration, Science Mission Directorate, Earth Science Technology Office, as part of the Instrument Incubator Program under grant NNX14AK70G. We acknowledge the support by the NASA-sponsored Jet Propulsion Laboratory (JPL), California Institute of Technology. An additional grant from JPL's Advanced Concept Funding enabled the development of the FMRS that was used in this study. We also thank the two anonymous reviewers for detailed and helpful comments. The data generated from this study are available upon request from the authors. Please contact the corresponding author at jonathan.h.jiang@jpl.nasa.gov.

References

Bennartz, R., and G. Petty (2001), The sensitivity of microwave remote sensing observations of precipitation to ice particle size distributions, *J. Appl. Meteorol.*, *40*, 345–364.

Buehler, S. A., et al. (2007), A concept for a satellite mission to measure cloud ice water path, ice particle size, and cloud altitude, *Q. J. R. Meteorol. Soc.*, *133*, 109–128.

Bony, S., et al. (2006), How well do we understand and evaluate climate change feedback processes?, *J. Clim.*, *19*, 3445–3482, doi:10.1175/JCLI3819.1.

Chen, W.-T., C. P. Woods, J.-L. F. Li, D. E. Waliser, J.-D. Chern, W.-K. Tao, J. H. Jiang, and A. M. Tompkins (2011), Partitioning CloudSat ice water content for comparison with upper tropospheric ice in global atmospheric models, *J. Geophys. Res.*, *116*, D19206, doi:10.1029/2010JD015179.

Elsaesser, G. S., A. D. Genio, J. H. Jiang, and M. van Lier-Walqui (2016), An improved convective ice parameterization for the NASA GISS global climate model and impacts on cloud ice simulation, *J. Clim.*, *30*, 317–336, doi:10.1175/JCLI-D-16-0346.1.

Evans, K. F. (2007), SHDOMPPDA: A radiative transfer model for cloudy sky data assimilation, *J. Atmos. Sci.*, *64*, 3854–3864, doi:10.1175/2006JAS2047.1.

Evans, K. F., S. J. Walter, A. J. Heymsfield, and M. N. Deeter (1998), Modeling of submillimeter passive remote sensing of cirrus clouds, *J. Appl. Meteorol.*, *37*, 184–205.

Evans, K. F., S. J. Walter, A. J. Heymsfield, and G. M. McFarquhar (2002), The submillimeter-wave cloud ice radiometer: Simulations of retrieval algorithm performance, *J. Geophys. Res.*, *107*(D3), 4028, doi:10.1029/2001JD000709.

Evans, K. F., J. R. Wang, D. O'C Starr, G. Heymsfield, L. Li, L. Tian, R. P. Lawson, A. J. Heymsfield, and A. Bansemer (2012), Ice hydrometeor profile retrieval algorithm for high-frequency microwave radiometers: Application to the CoSSIR instrument during TC4, *Atmos. Meas. Tech.*, *5*, 2277–2306, doi:10.5194/amt-5-2277-2012.

Fovell, R., and H. Su (2007), Impact of cloud microphysics on hurricane track forecasts, *Geophys. Res. Lett.*, *34*, L24810, doi:10.1029/2007GL031723.

Fu, Q., and K.-N. Liou (1993), Parameterization of the radiative properties of cirrus clouds, *J. Atmos. Sci.*, *50*, 2008–2025.

Golaz, J.-C., L. W. Horowitz, and H. Levy II (2013), Cloud tuning in a coupled climate model: Impact on 20th century warming, *Geophys. Res. Lett.*, *40*, 2246–2251, doi:10.1002/grl.50232.

Han, J., and H.-L. Pan (2011), Revision of convection and vertical diffusion schemes in the NCEP Global Forecast System, *Weather Forecasting*, *26*, 520–533, doi:10.1175/WAF-D-10-05038.1.

Hartmann, D. L., and D. A. Short (1980), On the use of earth radiation budget statistics for studies of clouds and climate, *J. Atmos. Sci.*, *37*, 1233–1250.

Heymsfield, A. J. (2003), Properties of tropical and midlatitude ice cloud particle ensembles. Part I: Median mass diameters and terminal velocities, *J. Atmos. Sci.*, *60*, 2573–2591.

Heymsfield, A. J., and C. Westbrook (2010), Advances in the estimation of ice particle fall speeds using laboratory and field measurements, *J. Atmos. Sci.*, *67*, 2469–2482, doi:10.1175/2010JAS3379.1.

Heymsfield, A. J., C. Schmitt, and A. Bansemer (2013), Ice cloud particle size distributions and pressure-dependent terminal velocities from in situ observations at temperatures from 0 to −86°C, *J. Atmos. Sci.*, *70*(12), 4123–4154.

Heymsfield, A. J., M. Krämer, N. B. Wood, A. Gettelman, P. R. Field, and G. Liu (2017), Dependence of the ice water content and snowfall rate on temperature, globally: Comparison of in situ observations, satellite active remote sensing retrievals, and global climate model simulations, *J. Appl. Meteorol. Climatol.*, *56*, 189–215, doi:10.1175/JAMC-D-16-0230.1.

Hong, Y., and G. Liu (2015), The characteristics of ice cloud properties derived from CloudSat and CALIPSO measurements, *J. Clim.*, *28*, 3880–3901, doi:10.1175/JCLI-D-14-00666.1.

Hong, S. Y., J. Dudhia, and S. H. Chen (2004), A revised approach to ice microphysical processes for the bulk parameterization of clouds and precipitation, *Mon. Weather Rev.*, *132*, 103–120.

Hong, S.-Y., Y. Noh, and J. Dudhia (2006), A new vertical diffusion package with an explicit treatment of entrainment processes, *Mon. Weather Rev.*, *134*, 2318–2341, doi:10.1175/MWR3199.1.

Huang, L., J. H. Jiang, Z. Wang, H. Su, M. Deng, and S. Massie (2015), Climatology of cloud water content associated with different cloud types observed by A-Train satellites, *J. Geophys. Res. Atmos.*, *120*, 4196–4212, doi:10.1002/2014JD022779.

Iacono, M. J., J. S. Delamere, E. J. Mlawer, M. W. Shephard, S. A. Clough, and W. D. Collins (2008), Radiative forcing by long-lived greenhouse gases: Calculations with the AER radiative transfer models, *J. Geophys. Res.*, *113*, D13103, doi:10.1029/2008JD009944.

Jiang, J. H., H. Su, C. Zhai, S. T. Massie, M. R. Schoeberl, P. R. Colarco, S. Platnick, Y. Gu, and K. N. Liou (2011), Influence of convection and aerosol pollution on ice cloud particle effective radius, *Atmos. Chem. Phys.*, *11*, 457–463, doi:10.5194/acp-11-457-2011.

Jiang, J. H., et al. (2012), Evaluation of cloud and water vapor simulations in CMIP5 climate models using NASA A-Train satellite observations, *J. Geophys. Res.*, *117*, D1410, doi:10.1029/2011JD017237.

Kangaslahti, P., E. Schlecht, J. Jiang, W. R. Deal, A. Zamora, K. Leong, S. C. Reising, X. Bosch, and M. Ogut (2016), CubeSat scale receivers for measurement of ice in clouds, in *2016 14th Specialist Meeting on Microwave Radiometry and Remote Sensing of the Environment (MicroRad)*, pp. 42-47, IEEE, Espoo, Finland, doi:10.1109/MICRORAD.2016.7530501.

Kroese, D. P., T. Taimre, and Z. I. Botev (2011), *Handbook of Monte Carlo Methods, Wiley Series in Probability and Statistics*, John Wiley, New York.

L'Ecuyer, T. S., and J. H. Jiang (2010), Touring the atmosphere aboard the A-Train, *Phys. Today*, *63*(7), 36–41, doi:10.1063/1.3463626.

Levenberg, K. (1944), A method for the solution of certain non-linear problems in least squares, *Q. Appl. Math.*, *2*, 164–168.

Li, J. F., et al. (2012), An observationally based evaluation of cloud ice water in CMIP3 and CMIP5 GCMs and contemporary reanalyses using contemporary satellite data, *J. Geophys. Res.*, *117*, D16105, doi:10.1029/2012JD017640.

Marquardt, D. (1963), An algorithm for least-squares estimation of nonlinear parameters, *SIAM J. Appl. Math.*, *11*(2), 431–441, doi:10.1137/0111030.

McFarquhar, G. M., and A. J. Heymsfield (1997), Parameterization of tropical cirrus ice crystal size distributions and implications for radiative transfer: Results from CEPEX, *J. Atmos. Sci.*, *54*, 2187–2200.

Morrison, H., and W. W. Grabowski (2008), Modeling supersaturation and sub-grid scale mixing with two-moment warm bulk microphysics, *J. Atmos. Sci.*, *65*, 792–812.

Morrison, H., G. Thompson, and V. Tatarskii (2009), Impact of cloud microphysics on the development of trailing stratiform precipitation in a simulated squall line: Comparison of one- and two-moment schemes, *Mon. Weather Rev.*, *137*, 991–1007.

Reising, S. C., et al. (2016), Tropospheric Water and cloud ICE (TWICE) millimeter and submillimeter-wave radiometer instrument for 6U-Class nanosatellites, in *2016 41st International Conference on Infrared, Millimeter, and Terahertz waves (IRMMW-THz)*, pp. 1–2, IEEE, Copenhagen, doi:10.1109/IRMMW-THz.2016.7758396.

Rodgers, C. D. (2000), *Inverse Methods for Atmospheric Sounding: Theory and Practice*, 238 pp., World Sci., River Edge, N. J., doi:10.1142/9789812813718_0004.

Sanderson, B. M., C. Piani, W. J. Ingram, D. A. Stone, and M. R. Allen (2008), Towards constraining climate sensitivity by linear analysis of feedback patterns in thousands of perturbed-physics GCM simulations, *Clim. Dyn.*, *30*, 175–190.

Skamarock, W. C., J. B. Klemp, J. Dudhia, D. O. Gill, D. M. Barker, W. Wang, and J. G. Powers (2008), A description of the Advanced Research WRF Version 3, *NCAR Tech. 16 Note TN-468+STR*, 113 pp.

Su, H., et al. (2017), Tightening of tropical ascent and high clouds key to precipitation change in a warmer climate, *Nat. Commun.*, doi:10.1038/ncomms15771.

Takahashi, H., H. Su, and J. H. Jiang (2016), Error analysis of upper tropospheric water vapor in CMIP5 models using "A-Train" satellite observations and reanalysis data, *Clim. Dyn.*, *46*, 2787–2803, doi:10.1007/s00382-015-2732-9.

Waliser, D. E., et al. (2009), Cloud ice: A climate model challenge with signs and expectations of progress, *J. Geophys. Res.*, *114*, D00A21, doi:10.1029/2008JD010015.

Wang, P. H., et al. (1996), A 6-year climatology of cloud occurrence frequency from Stratospheric Aerosol and Gas Experiment II observations (1985–1990), *J. Geophys. Res.*, *101*(D23), 29,407–29,429, doi:10.1029/96JD01780.

Wylie, D. P., D. L. Jackson, W. P. Menzel, and J. J. Bates (2005), Trends in global cloud cover in two decades of HIRS observations, *J. Clim.*, *18*, 3021–3031.

Wu, D. L., J. H. Jiang, and C. P. Davis (2006), EOS MLS cloud ice measurements and cloudy-sky radiative transfer model, *IEEE Trans. Geosci. Remote Sens.*, *44*(5), 1156–1165.

Wu, D. L., J. H. Jiang, W. G. Read, R. T. Austin, C. P. Davis, A. Lambert, G. L. Stephens, D. G. Vane, and J. W. Waters (2008), Validation of the Aura MLS cloud ice water content (IWC) measurements, *J. Geophys. Res.*, *113*, D15S10, doi:10.1029/2007JD008931.

Yang, P., L. Bi, B. A. Baum, K.-N. Liou, G. W. Kattawar, M. I. Mishchenko, and B. Cole (2013), Spectrally consistent scattering, absorption, and polarization properties of atmospheric ice crystals at wavelengths from 0.2 to 100 μm, *J. Atmos. Sci.*, *70*, 330–347, doi:10.1175/JAS-D-12-039.1.